Strength Reliability of Micro Polycrystalline Silicon Structure

Hamada, Shigeru
Department of Mechanical Engineering Science, Kyushu University

Hashizume, Kenji
Department of Mechanical and Aerospace Engineering, Kyushu University

https://hdl.handle.net/2324/8004

KYUSHU UNIVERSITY

Strength Reliability of Micro Polycrystalline Silicon Structure

by

Shigeru HAMADA[*] and Kenji HASHIZUME[**]

Abstract

In order to evaluate strength reliability of micron size polycrystalline silicon (poly-Si) structure for microelectromechanical systems (MEMS), bending strength tests of cantilever beam, Weibull analysis of the strength and fracture surface analysis are performed. Recently, the importance of MEMS in society is increasing, and the number of production is also increasing. MEMS devices, which contain mechanical movement, have to maintain their reliability in face of external shock, thermal stress and residual stress from manufacturing processes. When the age of the MEMS mass production comes, in case the material strength design of MEMS is performed, required strength data is not average value but the variation, especially minimum value assumed of the structure and material. Then, in order to evaluate strength reliability of micron size poly-Si structure, tests and analysis are performed. The specimen is made by chemical vapor deposition (CVD) process and the thickness is 3.5, 6.4 and 8.3 [μm] and the specimen has notch (stress concentration). The test specimen used for the test changed characteristics of (1) film thickness (2) stress concentration, and investigation about the influence each effect of the variation in a bending strength with fracture surface analysis are discussed.

Keywords: Polycrystalline silicon, Strength, Reliability, Stress concentration, Weibull analysis, Effective surface area

1. Introduction

Polycrystalline silicon (poly-Si) structure is widely employed in the Micro-Electro-Mechanical Systems (MEMS) [1, 2]. MEMS devices, which contain mechanical movement, have to maintain their reliability in face of external shock, thermal stress and residual stress from manufacturing processes, and fracture will begin mainly in stress concentration area. Therefore, it is necessary to build up reliability design criterion of the poly-Si structure that has stress concentration [3-9]. On the other hand, in mass production of MEMS products, it is also important to control the quality considering the reliability of poly-Si structure, which has scattered strength. Thus, we have to clarify the stress concentration effect on strength and the scatter of the strength of the poly-Si

[*]   Lecturer, Department of Mechanical Engineering Science
[**]   Undergraduate Student, Department of Mechanical and Aerospace Engineering

structure.   In order to clarify these subjects, bending tests using micro scale cantilever beams with or without notch of several sizes are performed.

2.   Test Method and Results
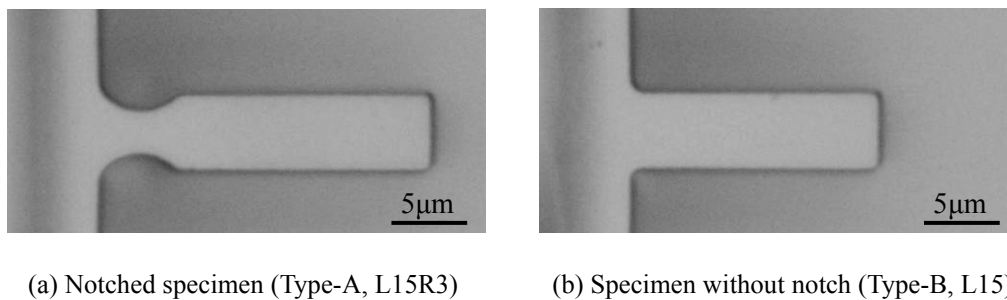
2.1 Specimen and test method

The specimens are illustrated in **Fig. 1**, and the photographs of specimens are shown in **Fig. 2**. Shapes and dimensions of the specimens are shown in **Table 1**.   For bending tests, two types of specimens; Type-A and B are prepared.   In the Type-A specimen, the notch of several sizes (1~5 [μm]) is introduced in the root section of micro-cantilever beam.   In the Type-B, by the microscopic observation, the 1μm corner radius is recognized indeed in the root section of microcantilever beam.   And the thickness of the specimen is 3.5, 6.4 and 8.3 [μm].

The poly-Si is chemical vapor deposited (CVD) on single crystal silicon wafer surface, and the specimens are made from surface micromachining process.   Manufacturing process of specimens is shown in **Fig. 3** schematically.   In order to reduce residual stress, the specimens are made of 4 poly-Si layers.   The gap between the cantilever and the substrate is 2 [μm].

A dynamic ultra micro hardness tester (Shimadzu Co. DUH-W201) with a Berkovich diamond indenter is used for the bending tests.   The test machine is for hardness test but we can obtain the relationship between load and displacement with satisfactory accuracy by this machine.   **Table 2** shows the properties of the test machine.   The test load speed is 1.421 [mN/sec.].   The bending tests are carried out at room temperature under the atmospheric environment.

(a) Notched specimen (Type-A)   (b) Specimen without notch (Type-B).
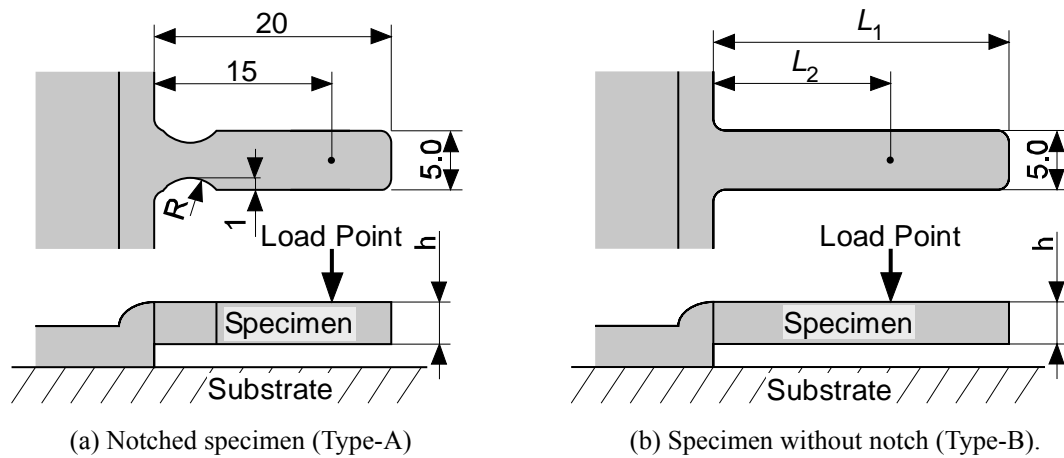
Fig. 1   Schematic diagram of the specimens (Unit: μm), h = 3.5, 6.4, 8.3[μm].

(a) Notched specimen (Type-A, L15R3)   (b) Specimen without notch (Type-B, L15)

Fig. 2   Optical microscope photograph on the surface of a test specimen.

Table 1   Shapes and dimensions of the specimen.

Specimen Type		L_1[μm]	L_2[μm]	R[μm]
Type-A	L15R1	20	15	1
	L15R2	20	15	2
	L15R3	20	15	3
	L15R4	20	15	4
	L15R5	20	15	5
Type-B	L10	15	10	-
	L15	25	15	-
	L30	35	30	-

Table 2   Properties of the test machine.

Load range	0.1 to 1961 [mN]
Minimum measurable load	0.2 [μN]
Indentation depth range	0 to 10 [μm]
Minimum measurable displacement	0.001 [μm]
Indenter	Tetrahedral Berkovich diamond
Tip radius of indenter	0.1 [μm] or less
Displacement measure method	Differential transformer
Loading method	Electromagnetic coil

(a) Initial

(b) Sacrificed layer deposition

(c) Poly-Si deposition

(d) Sacrificed layer release
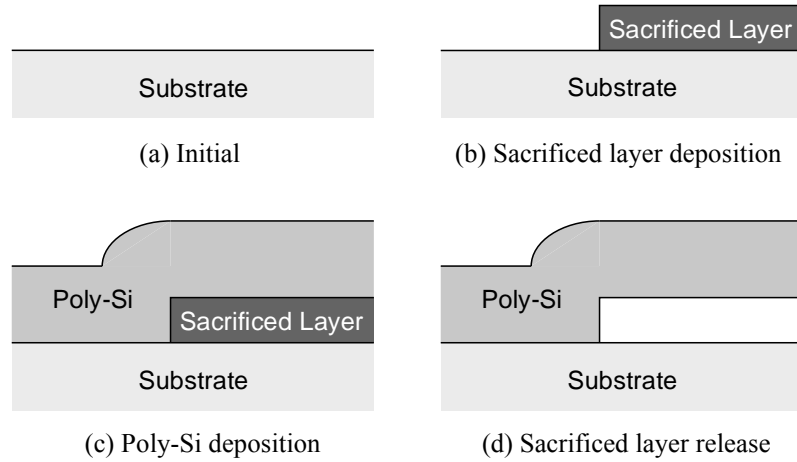
Fig. 3   Specimen making process (root section of cantilever).

2.2 FEM analysis

In order to quantify the fracture of specimens by the applied stresses in the tests, three-dimensional finite element elastic analyses are performed.   **Figure 4** indicates the examples of FEM models of the specimens (Type-A, L15R1).   For the Type-B specimen, the 1[μm] corner radiuses are taken into the model based on the microscopic observations mentioned above.   The stress concentration factor of Type-B is close to that of Type-A, L15R3.   The element sizes of the models are about 0.5[μm] in the overall region and are about 0.1[μm] in the stress concentration area around thee notch root.   The analyses are carried out under the load condition such as the displacement of loading point is equal to 1[μm].   **Table 3** and **Table 4** show the FEM analysis conditions and material properties respectively.

(a) Whole of the FEM model (1/2 model)   (b) Detail of the stress concentration (notch) section of the specimen
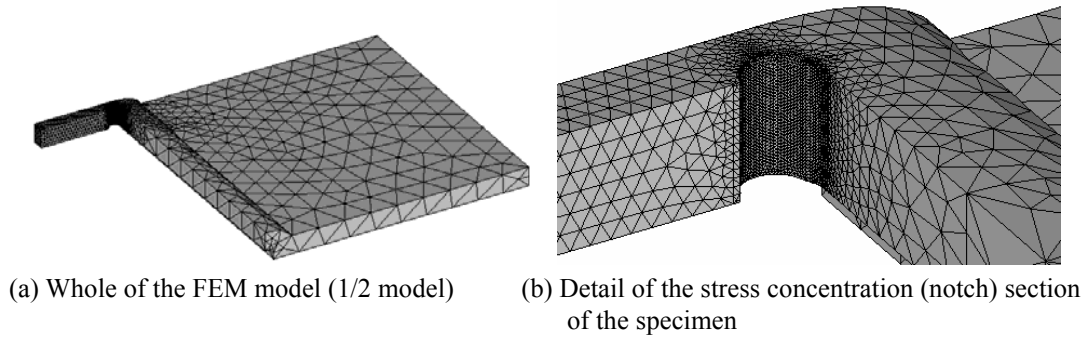
Fig. 4   Examples of the FEM model (L15R1).

Table 3   FEM analysis conditions.

|	
Elements	3-dimensional 10-node Tetrahedral
Solver	ANSYS 10.0
Load condition	1 [μm] displacement on the load point
Number of elements	About 8,400

Table 4   Material properties for FEM analysis.

Young's modulus	148 [GPa]
Poisson's ratio	0.2 [-]

$h = 6.4$μm, $R = 1$μm
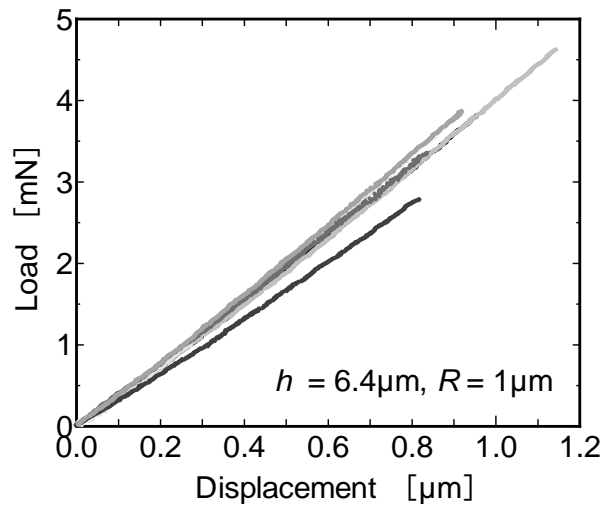
Fig. 5   Example of relationship between load and displacement (Specimen type: L15R1).

2.3 Test results

Figure 5 shows examples of the relationship between load and displacement of the bending tests.   In this figure, it is known that the polycrystalline silicon deformed elastically until final catastrophic failure in room temperature, showing a brittle nature.   The relationship between load and displacement shows a little nonlinear behavior.   This is because of indentation to poly-Si of the indenter.
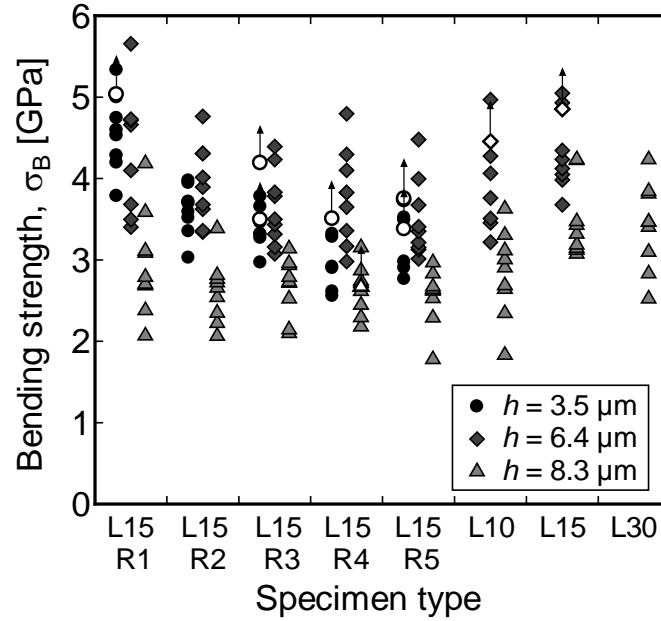
Fig. 6   Relationship between maximum stress in notch root and specimen type.

Figure 6 shows an expression of the test results by use of maximum peak stress σ_{max} in the notch root obtained by FEM analysis.   In this figure, the plots of solid mark means the data of fracture specimens and the open mark means the data of non-fracture specimens due to the contact of free edge to the substrate surface before break.   The displacement which contact occur changes with specimen, this may be because the residual stress and shape of the specimens has little difference respectively.   In **Fig. 6,** a tendency can be seen that the plots by the σ_{max} move down with the increase in notch radius because of the effect of the difference on the stress distribution pattern.

3.   Discussion

3.1 Weibull parameters

Figure 7 shows the Weibull plots of bending strength for poly-Si.   The non-fracture data are treated statistically [10].   **Figure 7** show the validity of using Weibull analysis for this study.

Figure 8 shows the scale parameters (β) of this study.   If shapes of the specimen are different, then effective surface area is different.   Then, the scale parameter is thought to be different. **Figure 8**(a) shows the validity of the effective surface.   **Figure 8**(b) shows the same result.   In **Fig.8**, h = 3.5[μm] specimen shows different trend.   We'll discuss about it later.

Figure 9 shows the result of shape parameter (α).   With effective surface area, Weibull parameters (α, β) are shown as follows.
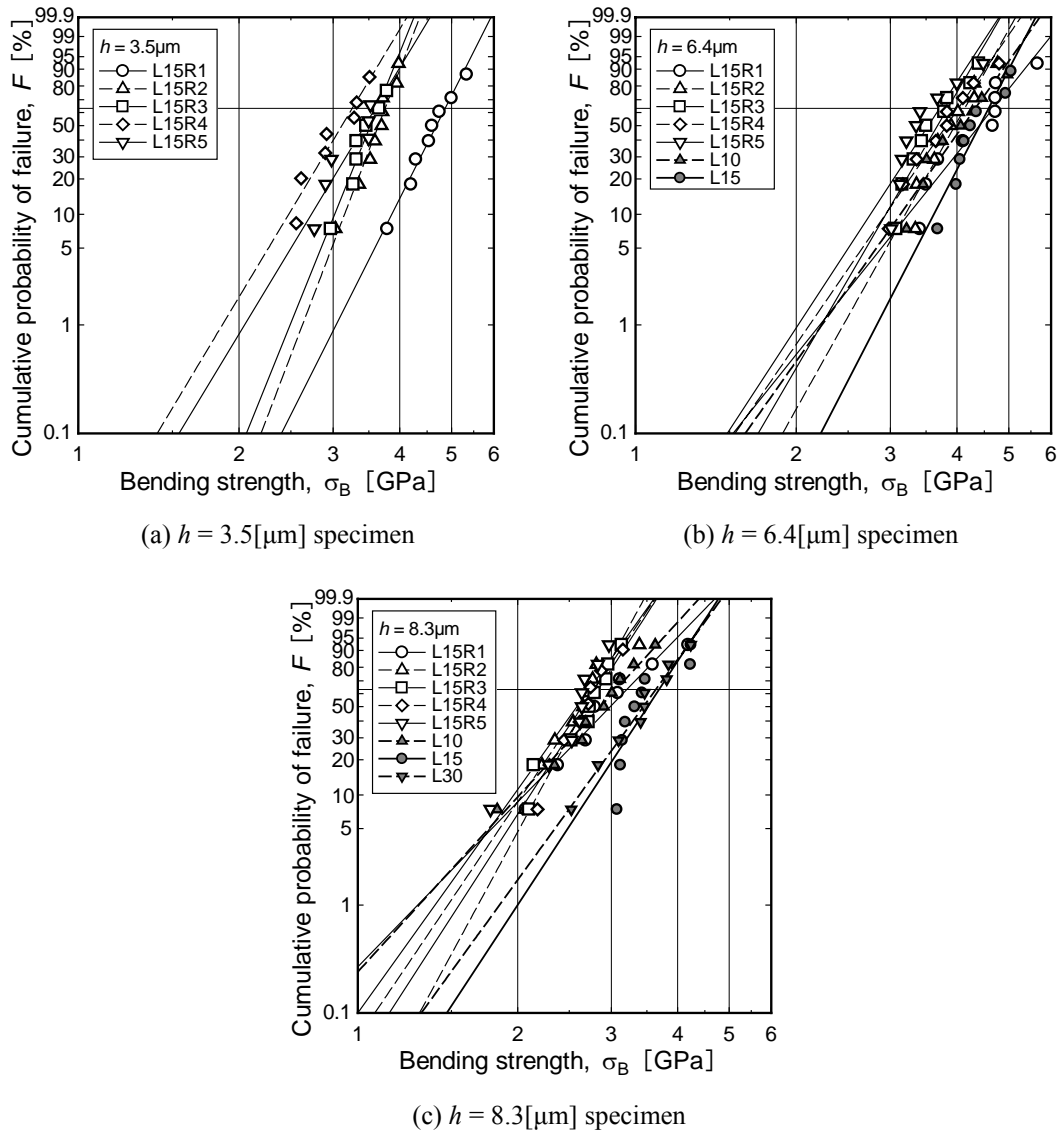
$$F = 1 - \exp\left\{-A_E\left(\frac{\sigma}{\beta}\right)^{\alpha}\right\} \tag{1}$$

where F is the fracture probability, σ is the applied stress and A_E is the effective surface area that is the area of the tested part.   For Weibull plots, Eq. (1) is changed as follows.
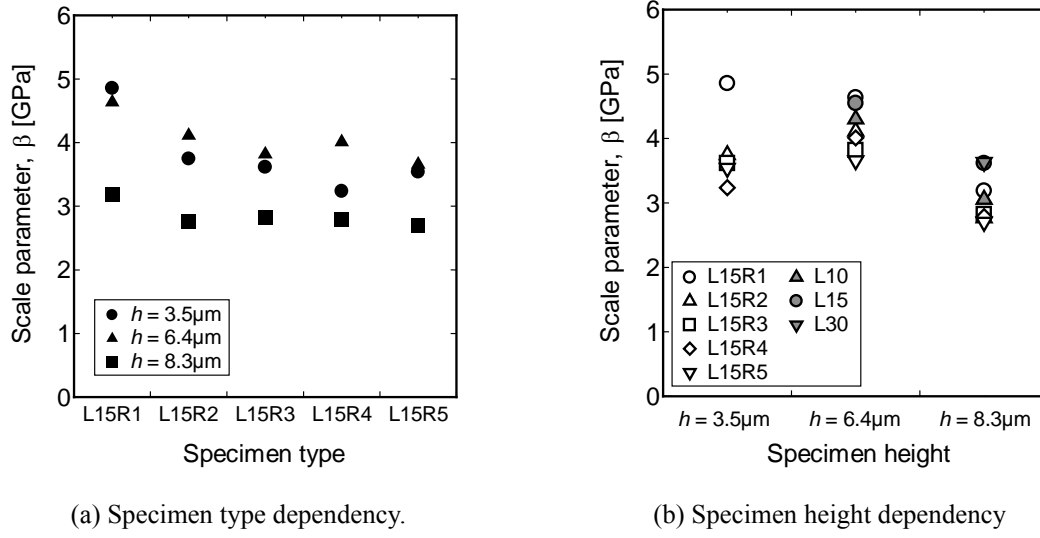
$$\ln \ln \frac{1}{1-F} = \alpha \left(\ln \sigma - \ln \beta \right) + \ln A_E \tag{2}$$

Eq. (2) shows the shape parameter (α) is independent of the effective area (A_E). Therefore, the shape parameter is the same when strength scattering is the same material, though effective areas (A_E) differ (specimen thickness differ).

In **Fig.9**, though h = 6.4 and 8.3[μm] specimen show almost same shape parameter (α), h = 3.5[μm] specimen show different shape parameter (α). Therefore, it turns out that the material used for the h = 3.5[μm] specimen has different strength scattering from the material of other specimens.

(a) h = 3.5[μm] specimen

(b) h = 6.4[μm] specimen

(c) h = 8.3[μm] specimen

Fig. 7   Weibull plots of bending strength for poly-Si.

(a) Specimen type dependency.   (b) Specimen height dependency

Fig. 8   Scale parameters of the bending strength for poly-Si.
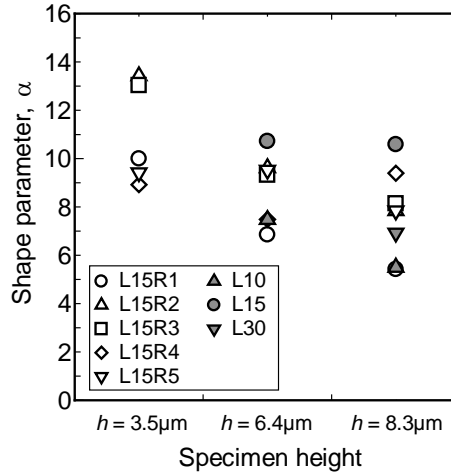

Fig. 9   Shape parameters of the bending strength for poly-Si.

Figure 10 shows the fracture surface and around the fracture surface of poly-Si of this study. **Fig.10** (a) (h = 3.5[μm]) are different from **Fig.10** (b, c) (h = 6.4, 8.3[μm]).   This is because the etching processes for these specimens are different.   Specimen h = 6.4[μm] and 8.3[μm] are made by same DRIE (Deep Reactive Ion Etching) process, but h = 3.5[μm] is made by another RIE (Reactive Ion Etching) process.   Then the side surface condition of these specimen (material) are different and the shape parameters (α) become different between h = 3.5[μm] specimen and h = 6.4, 8.3[μm] specimen.

Figure 11 shows a fracture surface that fracture origin can be found.   River line pattern[11] can be seen on the fracture surface like other brittle materials.   By river line pattern, the origin of the fracture surface is clearly shown in this picture.   The fracture origin is located in side surface and not upper surface of the specimen.   This is because the effect of the surface conditions.

(a) h = 3.5[μm], L15R3.
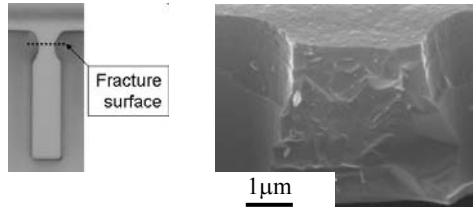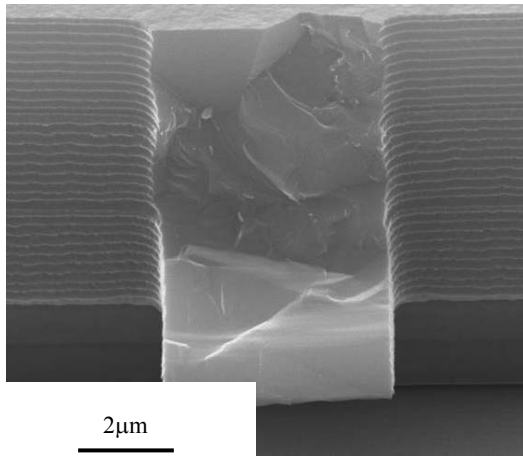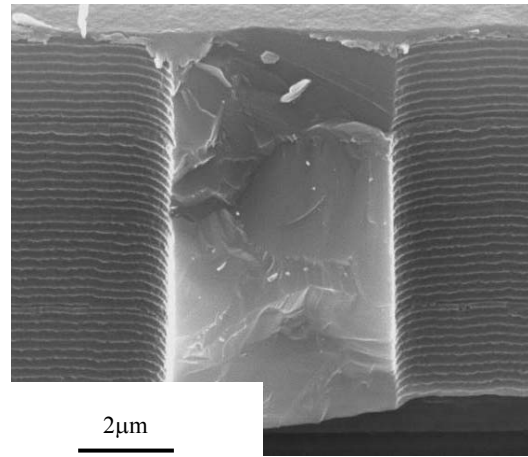
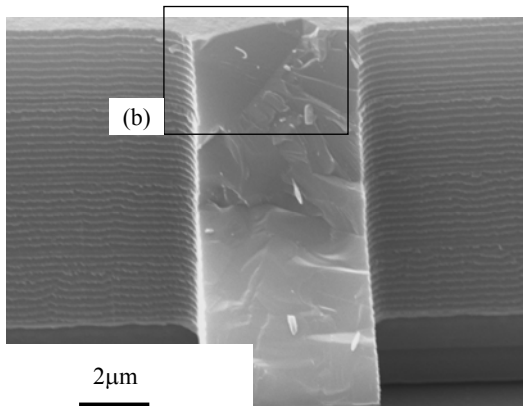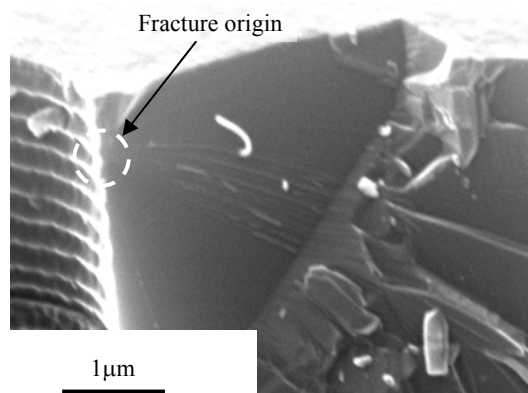(b) h = 6.4[μm], L30.   (c) h = 8.3[μm], L15.

Fig. 10   Fracture surface and surface image of poly-Si for this study.

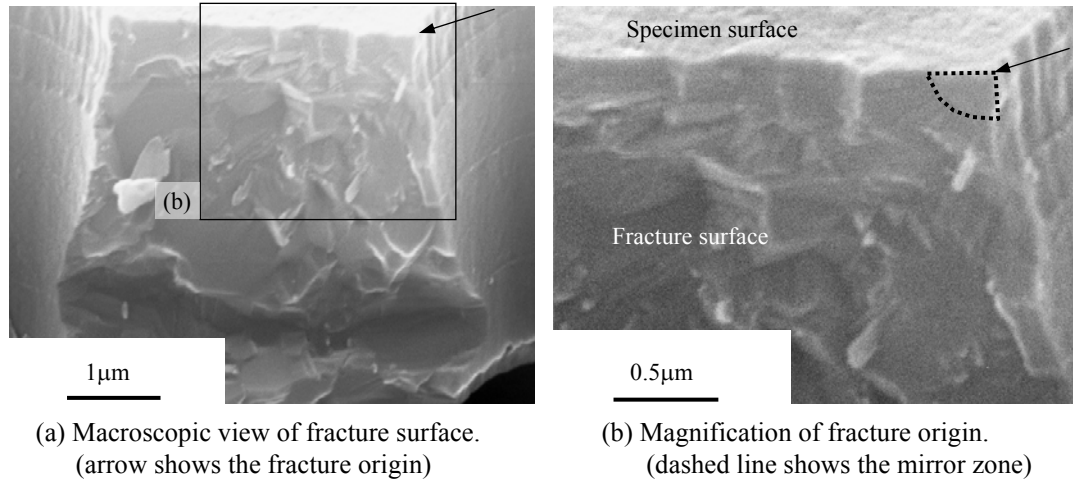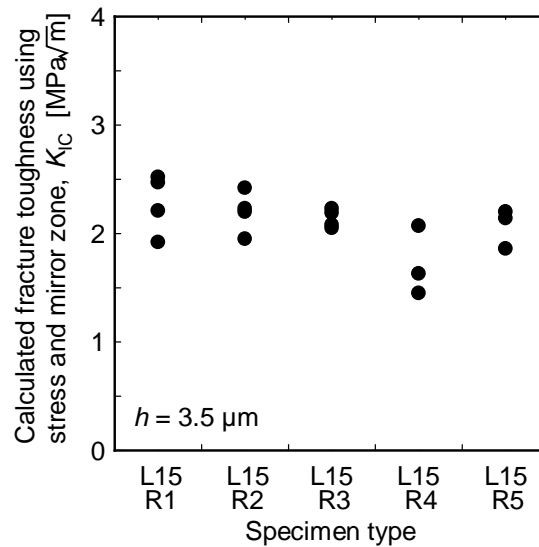(a) Whole fracture surface   (b) Magnification of fracture origin

Fig.11   Fracture origin on the side surface of the cantilever specimen (h = 8.3[μm], L30).

3.2 Fracture toughness

In order to make clear the reason of the strength scattering, analysis of the fracture surface by SEM (Scanning Electron Microscope) are performed.   If the variation of the strength is dependent on the initial defect size, then calculated fracture toughness is thought to be same.   **Figure 12** show one example of the analysis.   In this figure, in the area of fracture origin, a mirror zone [11] came under observation.   Then, we assume that the mirror zone is initial defect, stress intensity factors for the mirror zone are calculated by quarter-elliptical crack in a plate under bending mode stress distribution[12].   **Figure 13** shows the results.   The average of the fracture toughness is 2.1 [MPa$\sqrt{}$m].   **Table 5** shows reported fracture toughness (K_{IC}) of poly-Si[13-16] and single crystal Si[17].   Then the value found to be about double.   Then area of mirror zone is not same as area of initial defect.   But **Fig.13** shows that the fracture toughness is independent on specimen shape and the value is constant to some extent.   Then area of mirror zone assumed to be proportional to the initial defect.

(a) Macroscopic view of fracture surface.
(arrow shows the fracture origin)

(b) Magnification of fracture origin.
(dashed line shows the mirror zone)

Fig. 12   Example of fracture surface (h = 3.5[μm], L15R3).

**Fig. 13**   Scale parameters of the bending strength for poly-Si.

Table 5 Reported fracture toughness (K_{IC}) of Poly-Si and single crystal Si.

Ref.	Material	Measured K_{IC} [MPa√m]	Load	Pre-crack
13)	Poly-Si	1.0	Tensile	Vickers indentation
14)	Poly-Si (B-doped)	1.5	Tensile	Fatigue crack
	Poly-Si (P-doped)	1.7	Tensile	Fatigue crack
15)	Poly-Si	1.00±0.1	Tensile	Vickers indentation
16)	Poly-Si	0.843-1.225	Tensile	Vickers indentation
17)	Single crystal Si {111} orientation	0.82	Bending	Knoop indentation
	Single crystal Si {110} orientation	0.90	Bending	Knoop indentation
	Single crystal Si {100} orientation	0.95	Bending	Knoop indentation

3.3 Fracture angle

More fractographic analysis is performed.   Then, we found that the angle of mirror zone is different from the principal stress surface.   An example of the observation result and the definition of the angle (θ) are shown in **Fig.14**.   **Figure 15** shows the relationship between fracture toughness using stress and mirror zone and the angle.   In this figure dependency of the fracture toughness on the angle can be seen.   The reasons are thought as follows. (1) The poly-Si crystal on the fracture origin area are different from principal stress direction (2) the poly-Si grain boundary on the fracture initiation area are different from principal stress direction.
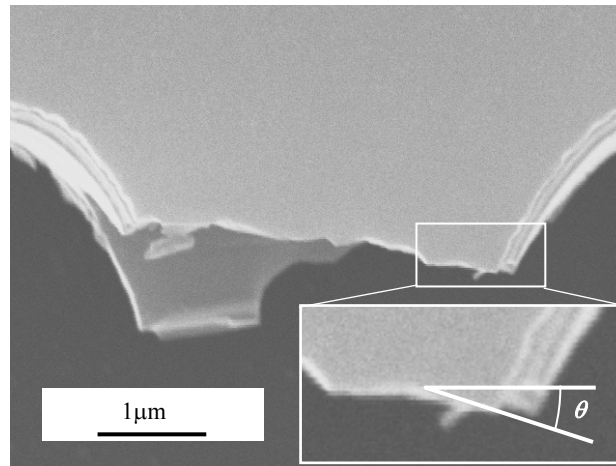
Fig. 14   Definition of fracture surface (mirror zone) angle.
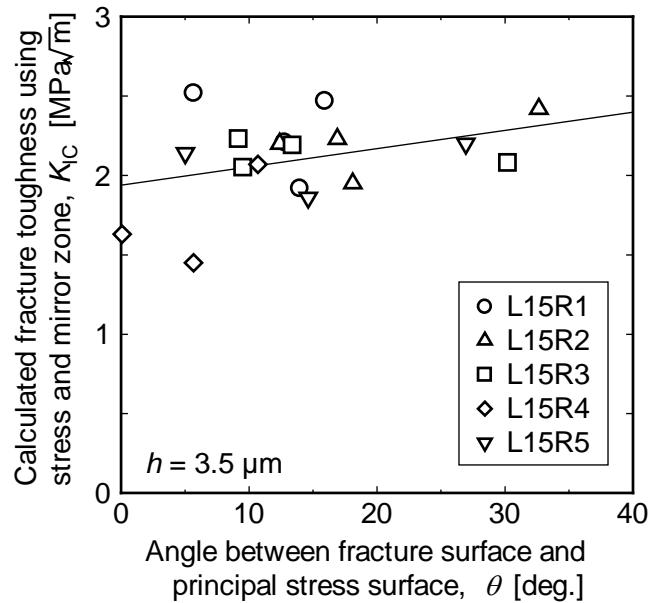
Fig. 15   Angle dependency of fracture toughness.

4.   Conclusions

In order to evaluate strength reliability of micron size polycrystalline silicon (poly-Si) structure, bending tests of cantilever beam, Weibull analysis and fracture surface analysis are performed. The test results are concluded as follows.

(1)   By Weibull analysis, we found that the scatter in poly-Si bending strength made by RIE process is smaller than that of DRIE process.

(2)   Effective surface area can be used for the strength of poly-Si structure qualitatively.

(3)   Poly-Si strength is scattered. It depends on surface condition, crystal or grain boundary direction and some other.

References

1)   S. D. Senturia, Microsystem Design, Kluwer Academic Publishers, Dordrecht (2000).

2)   K. Najafi, Micromachined Micro Systems: Miniaturization Beyond Microelectronics, Proc. 2000 Symposium on VLSI Circuits Digest of Technical Papers, pp.6-13 (2000).

3)   S. Greek, F. Ericson, S. Johansson and J.-Å. Schweitz, In situ tensile strength measurement and Weibull analysis of thick film and thin film micromachined polysilicon structures, Thin Solid Films, Vol.292, pp.247-254 (1997).

4)   T. Tsuchiya, O. Tabata, J. Sakata and Y. Taga, Specimen size effect on tensile strength of surface-micromachined polycrystalline silicon thin films, IEEE J. microelectromechanical systems, Vol.7, No.1, pp.106-113 (1998).

5)   T. Namazu, Y. Isono and T. Tanaka, Evaluation of size effect on mechanical properties of single crystal silicon by nanoscale bending test using AFM, IEEE J. microelectromechanical

systems, Vol.9, No.4, pp.450-459 (2000).

6) H. Kapels, R. Aigner and J. Binder, Fracture strength and fatigue of polysilicon determined by a novel thermal actuator, IEEE Trans. Electron Devices, Vol.47, No.7, pp.1522-1528 (2000).

7) W. N. Sharpe Jr., K. M. Jackson, K. J. Hemker and Z. Xie, Effect of specimen size on Young's modulus and fracture strength of polysilicon, IEEE J. microelectromechanical systems, Vol.10, No.3, pp.317-326 (2001).

8) K. S. Chen, A. A. Ayón, X. Zhang and S. M. Spearing, Effect of process parameters on the surface morphology and mechanical performance of silicon structures after deep reactive ion etching (DRIE), IEEE J. microelectromechanical systems, Vol.11, No.3, pp. 264-275 (2002).

9) C. L. Muhlstein, R. T. Howe and R. O. Ritchie, Fatigue of polycrystalline silicon for microelectromechanical system applications: crack growth and stability under resonant loading conditions, Mechanics of Materials, Vol.36, pp.13-33 (2004).

10) L. G. Johnson, The Statistical Treatment of Fatigue Experiments, Elsevier, New York (1964).

11) D. Hull, Fractography, Cambridge University Press, Cambridge, pp.91-129 (1999).

12) Y. Murakami Eds., Stress Intensity Factors Handbook Vol.3, Soc. Materials Sci., Japan & Pergamon Press, pp.591-597 (1992).

13) H. Kahn, N. Tayebi, R. Ballarini, R. L. Mullen and A. H. Heuer, Fracture toughness of polysilicon MEMS devices, Sensors and Actuators A, Vol.82, pp.274-280 (2000).

14) D. Son, J. Kim, T. W. Lim and D. Kwon, Evaluation of fracture properties of silicon by combining resonance frequency and microtensile methods, Thin Solid Films, Vol.468, pp.167-173 (2004).

15) I. Chasiotis, S. W. Cho and K. Jonnalagadda, Fracture toughness and subcritical crack growth in polycrystalline silicon, Trans ASME J. Applied Mechanics, Vol.73, pp.714-722 (2006).

16) S. W. Cho and K. Jonnalagadda and I. Chasiotis, Mode I and mixed mode fracture of Polysilicon for MEMS, Fatigue Fract. Engng. Mater. Struct., Vol.30, pp.21-31 (2007)

17) C. P. Chen and M. H. Leipold, Fracture toughness of silicon, American Ceramic Society Bulletin, Vol.59, No.4, pp.469-472 (1980).